Earthquake Geotechnical Engineering for Protection and Development of Environment and Constructions – Silvestri & Moraci (Eds)
© 2019 Associazione Geotecnica Italiana, Rome, Italy, ISBN 978-0-367-14328-2

A new simple neural-network based approach to predict the seismic response of levees and small height earth dams

C. Durand, E. Chaljub & P.Y. Bard
Institut des Sciences de la Terre, Grenoble, France

J.J. Fry
Electricite de France, Le Bourget-du-Lac, France

R. Granjon
Compagnie Nationale du RhOne, Lyon, France

E. Renalier
geophyConsult, Chambery, France

ABSTRACT: The issue of the seismic stability of embankments has been raised by several recent events. Given their very large cumulated length, together with the large variability of their owners, it is rarely possible to perform detailed investigations and complex numerical simulations, especially in moderate seismicity areas. Analyzing their capacity to withstand seismic loading thus requires the use of simple tools, based on a few easily available parameters. This work aims at providing an easy-to-use tool to assess peak acceleration at crest of embankments and peak acceleration of potential sliding blocks then allowing to evaluate their stability in case of earthquake. It is based on a 2D numerical parametric study combining 135 realistic configurations of embankments and natural soil layers, and four loading levels, characterized by peak acceleration at outcropping bedrock (0.0981 m/s^2, 0.981 m/s^2, 2.943 m/s^2 and 4.905 m/s^2 that correspond respectively to 0.01g, 0.1g, 0.3g and 0.5g). For each configuration and loading level, nonlinearity is taken into account by using equivalent shear modulus and damping consistent with the strain level (derived from a set of 1D linear equivalent computations). Artificial neural networks are then used to identify the parameters that best control the seismic response of the embankment while being easily available. They also provide a relation between these input parameters and the researched outputs (peak accelerations at embankment crest and for potential sliding blocks). A few abacus based on those neural networks are also provided as a visual tool to help engineers understanding the main trends.

1 INTRODUCTION

Levees, embankments along rivers and channels and small height earth dams are strategic facilities that must remain stable in case of earthquake. However, given the very large length of these structures, it is rarely possible to conduct complex numerical models for each section of the embankments in regions of moderate seismicity. It is interesting, if not mandatory, to develop simple tools in order to identify the weakest sections where more complex simulations are needed and to save money and time. The work of Durand et al. (2017) has shown the limitations of existing simplified methods and, in particular, the necessity of basing the simplified tools on realistic models that take into account the presence of natural soil below the embankment (generally located in alluvial valleys) and a correct energy dissipation. In this work, we

provide a new physics-based simplified tool to assess peak acceleration at crest of embankments and peak acceleration of potential sliding blocks.

2 NUMERICAL SIMULATIONS

A 2D numerical parametric study is first performed in order to evaluate the principal mechanisms that most influence the motion of the levee. These numerical computations also lead to the creation of the database required for the development of a predictive simplified tool. Numerical models have to be both realistic (in order to take into account the main phenomenon that influence the motion of an embankment) and relatively simple (in order to consider many situations and to be able to derive a simplified tool).

2.1 *Considered situations*

A numerical parametric study is performed to evaluate the seismic response of a large set of realistic embankments spanning a wide range of geometrical and mechanical properties. As illustrated in Figure 1(a), each model represents a symmetrical, trapezoidal embankment resting on a horizontal layer of soil; the bedrock is reached below this layer. The embankment is considered homogeneous, whereas the effect of confining pressure on mechanical properties is taken into account in the soil layer through a velocity gradient expr essed as a function of the depth z (z = 0 m corresponds to the top of the layer) as follows:

$$V_S(z) = V_a + (V_b - V_a)\sqrt{\frac{z - z_a}{z_b - z_a}} \tag{1}$$

where V_a and V_b are the shear wave velocities at elevations z_a = 0 m and z_b = -1000 m respectively. Furthermore, in each point of the soil layer, the additional confining pressure due to the presence of the embankment can be converted into an increment of the depth (that can be re-injected in equation 1 to get an increment of V_S). This increment Δ_z is determined using the solution from Flamant(1892), and can be expressed as follows

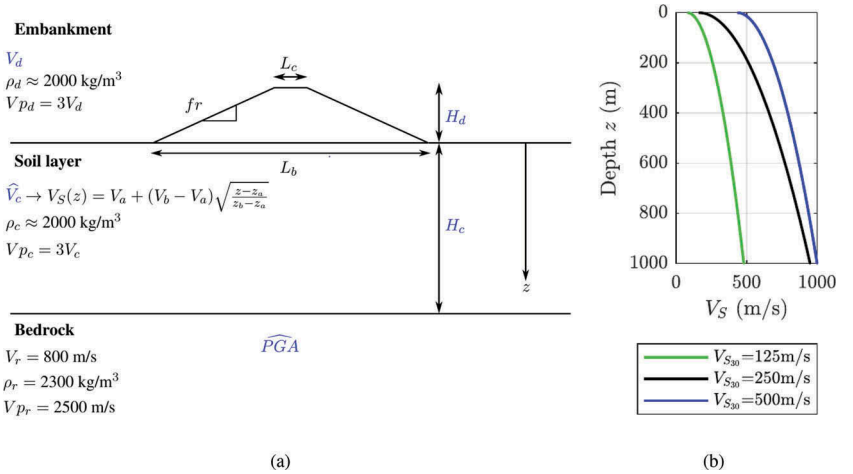

Figure 1. Description of the considered 2D numerical models: (a) 2D configurations of embankments and soil layers considered in the parametric study; (b) Shear waves velocity profiles $\hat{V}_c$ considered in the soil layer with corresponding Vs_{30} anchor values.

$$\Delta_z = \frac{\rho_d}{\rho_c}\frac{H_d}{\pi}\Theta \tag{2}$$

where ρ_d is the mass density in the embankment, ρ_c is the mass density in the layer, H_d is the embankment height and Θ is the angle formed between the point of the layer where the increment is calculated and the two extremities at the base of the embankment.

In the embankment and the soil layer, the velocity of P-waves is equal to three times the S-waves velocity and the mass density is equal to 2000 kg/m^3. In the bedrock, the S-waves velocity is taken equal to 800 m/s, the P-waves to 2300 m/s, and the unit mass to 2500 kg/m^3.

In total, 540 different numerical models are considered, characterized by five parameters (represented in blue in Figure 1(a)):

- the height of the embankment H_d (the crest width L_c, its width over height ratio fr and its base width L_b are adapted in function H_d in order to consider realistic sections of embankments);
- the thickness of the soil layer H_c;
- the shear waves velocity in the embankment V_d;
- the shear waves velocity profile in the soil layer (designated by $\hat{V}_c$), corresponding to different values of V_{S30}, that depends on the values of V_a and V_b in Equation 1;
- the loading level characterized by the peak acceleration at outcropping bedrock, referred to $\widehat{PGA}$ as in this paper.

The values taken by the parameters are given in Table 1. The velocity profile $\hat{V}_c$ given in this table corresponds to the values of V_{S30} of the three velocity profiles shown on Figure 1. These profiles are defined by Equation 1 using the values of V_a and V_b given in Table 1.

As listed in Table 1, 9 different embankments (3 geometries and 3 shear wave velocities), 15 foundation soil layers (5 thicknesses and 3 velocity profiles) and 4 loading levels (corresponding to the 4 values of $\widehat{PGA}$ - the value of 0.0981 m/s^2 accounting for the linear case) are taken into account in this parametric study.

The seismic response of the resulting 540 configurations is computed for 8 different input waveforms. Each of them is derived from real horizontal recordings of the RESORCE database (Akkar et al. 2014) obtained on outcropping rock sites, and then tuned to EC8-based French design spectra using a phase-keeping matching technique ((see Causse et al. 2014)). Each accelerogram is scaled to the desired value of *PGA* for the considered model.

2.2 *2D viscoelastic simulations*

The 2D spectral-element solver SPECFEM2D (Martin et al. 2008) is used for the direct numerical computation of the seismic response of the embankment. The code implements the spectral element method in space, with a polynomial order N=4, and a second order explicit finite-difference method in time. The total width of the computational domain is 4000 m, with the embankment in the middle, and it extends to a depth of -1500 m. The spectral element mesh is made of quadrangles. The mesh resolution is adapted to the shear wavelength in order to ensure that the results can be acceptable until 25 Hz. In all models, the input motion is introduced as a plane wave with vertical incidence, imposed at the elevation -1200 m. The

Table 1. Variation ranges of the input parameters considered in the paper. The total number of configurations is 540.

Geometries	*Hd (m)*/*Lc(m)*/*fr*/L_b (m) *Hc* (m)	4/4/1.5/16 - 10/6/2.5/56 - 20/10/3/130 3 - 10 - 30 - 100 - 300
Mechanical properties	*Vd* (m/s)	200 - 300 - 500
	Velocity profile VC (m/s) (v_{S30}/v_a/v_b)	125 $_{(125/80/480)}$ - 25 0 $_{(250/160/950)}$ - 5 00 $_{(500/434/1000)}$
Loading levels	$\widehat{PGA}$ (m/s^2)	0.0981 -0.981 -2.943 -4.905

polarization of the imposed motion coincides with the horizontal in-plane direction (SV wave). The impulse response of the 540 models is computed up to a frequency of 25 Hz, and then convolved with the 8 accelerograms.

In order to account for nonlinear energy dissipation in these 2D viscoelastic models, mechanical properties - that are specified at each point of the mesh - correspond to equivalent shear modulus and damping. These equivalent parameters are estimated by a large set of 1D linear equivalent simulations as described hereinafter.

2.3 *ID linear equivalent simulations*

The 2D models are discretized into a succession of 1D vertical columns of soil for which linear equivalent response are performed. Thus, 495 soil columns and the 8 chosen accelerograms are considered for 1D linear equivalent computations in SHAKE92 (Idriss & Sun 1992). The evolution of shear modulus and damping is supposed to follow the curves from Darendeli (2001) considering a plasticity index of 0%. These curves allow a dependence of degradation with confinement pressure (i.e. depth) which is really significant for the large depth soil columns. For each column, the mean equivalent damping and shear modulus derived from the 8 input waveforms is used in the 2D models where this"local 1D column"is encountered.

3 AMPLIFICATIONS AT CREST AND OF POTENTIAL SLIDING BLOCKS

For each of the 540 cases, the dynamic response of the embankment is characterized by the values of peak horizontal acceleration at crest, named $a_{crest_{\max}}$ (540 values), and peak horizontal acceleration of five potentially sliding blocks, named $a_{blockmax}$ (540 x 5 = 2700 values) - both correspond to mean results calculated on the 8 chosen accelerograms. The geometries of the blocks are presented on Figure 2. Each block is characterized by its maximum depth y_b normalized by the height of the embankment H_d that can take the following values: 1/4 (for the more superficial block), 1/2, 3/4, 1 and $\frac{H_d+3}{H_d}$ (for the deepest block). Each sliding block is considered to have a horizontal tangent at its lowest point.

These peak accelerations are characterized in a dimensionless way by their ratio to the peak acceleration at outcropping bedrock. They range from 0.19 (for a thick, soft soil and dyke, strong loading case: H_d = 20m, H_c = 100m, $\hat{V}_c$ = 125m/s, V_d = 200m/s, $\widehat{PGA}$ = 4.905m/s^2) to 4.22 (for a thin, stiff soil, soft dyke, low loading case:H_d = 10m, H_c = 3m, VC = 500m/s, V_d = 200m/s, $\widehat{PGA}$ = 0.0981m/s^2). Its (geometrical) mean value is equal to 1.23 with a logarithmic standard deviation 0.74 which corresponds to a multiplying or dividing factor 2.09. Similarly, the peak acceleration amplification ratios for potentially sliding blocks also span a wide range of values, from 0.18 (deep slide, thick soft soil, strong loading case: H_d = 20m, H_c = 100m, $\hat{V}_c$ = 125m/s, V_d = 300m/s, $\widehat{PGA}$ = 4.905m/s^2, y_b/H_d = 1.25) and 3.7 (shallow slide, thin and stiff soil, stiff dyke, low loading case: H_d = 10m, H_c = 10m, $\hat{V}_c$ = 500m/s, V_d = 200m/s, $\widehat{PGA}$ = 0.0981m/s^2, y_b/H_d = 0.33). Its mean value is equal to 1.01 with a logarithmic standard deviation 0.66 which corresponds to a multiplying or dividing factor 1.94.

In order to better understand the different physical mechanisms that control the amplification at crest, the amplitude of the ratio $\frac{a_{crest_{max}}}{\widehat{PGA}}$ is displayed in Figure 3 with a dedicated

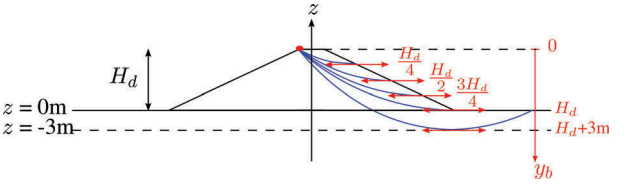

Figure 2. Geometries of the five possible sliding blocks considered.

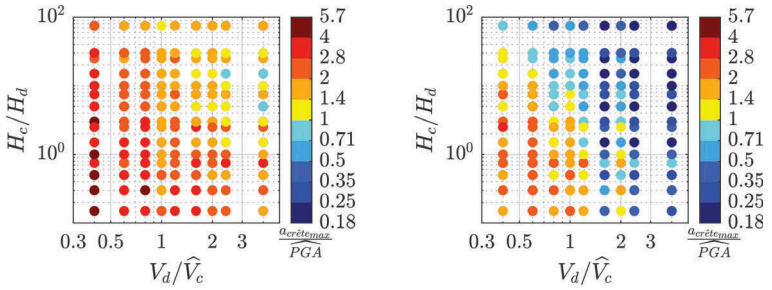

(a) $\widehat{PGA} = 0.0981\text{m/s}^2$. (b) $\widehat{PGA} = 4.905\text{m/s}^2$.

Figure 3. Amplitude of the ratio $a_{crest_{max}}/\widehat{PGA}$ in the plane formed by $V_d/\hat{V}_c$ and H_c/H_d in the (a) linear case ($\widehat{PGA} = 0.0981\text{m/s}^2$) (b) strongly nonlinear case ($\widehat{PGA} = 4.905\text{m/s}^2$).

colorscale in the plane formed by $V_d/\hat{V}_c$ and H_c/H_d for a given loading level $\widehat{PGA}$. The chosen parameters used to represent the amplification ratio at crest are similar to the adimensional parameters proposed by Sarma (1979) that are the impedance contrast and contrast in travel times of S-waves in the embankment and in the soil layer. Figure 3(a) considers the case of small deformations (linear case for a low value of $\widehat{PGA}$). In this situation, acceleration at crest is generally greater than at outcropping bedrock. Amplification is particularly strong when the embankment is softer than the soil layer. This situation favors the trapping of waves in the embankment and thus the occurence of topographical site effects. When the soil layer is soft (higher values of $Vd/\hat{V}_c$), the amplification is mainly due to 1D site effect in the soil layer. The strong influence of nonlinearity on peak acceleration at crest is visible in Figure 3(b): the value of $\frac{a_{crest_{max}}}{\widehat{PGA}}$ is systematically smaller than in the linear case, especially for soft and thick soil layers (high values of $V_d/\hat{V}_c$ and H_c/H_d) that allow large energy dissipation. It is important to notice that, even if Figure 3 shows some trends in the evolution of $\frac{a_{crest_{max}}}{\widehat{PGA}}$ with the parameters $V_d/\hat{V}_c$, H_c/H_d and $\widehat{PGA}$, it is not possible to identify on this figure a simple relation between the value taken by $\frac{a_{crest_{max}}}{\widehat{PGA}}$ and the three considered parameters.

Similar results are also obtained for the sliding blocks, as detailed in Durand (2018). The results shows that $a_{block_{max}}$ is generally smaller than $a_{crest_{max}}$, in particular when topographic effects are important and when the block is deep. In this case, amplification of peak acceleration is located near the crest; therefore, averaging the acceleration on a deep block necessarily leads to a smaller mean peak acceleration of the block compared with peak acceleration at crest.

4 PREDICTIVE MODEL BASED ON NEURAL NETWORK APPROACH

As shown previously (see Figure 3), values of the ratio $\frac{a_{crest_{max}}}{\widehat{PGA}}$ (and $\frac{a_{block_{max}}}{\widehat{PGA}}$) obtained from the numerical computations detailed above exhibit a complex, non-linear relationship between the parameters H_d, V_d, H_c, $\hat{V}_c$, $\widehat{PGA}$ (and y_b). In order to develop simple prediction tools, the main parameters (or combination of parameters) that best control the values of the researched ratio have first to be identified. The next step is to develop a model to approximate the complex dependence that links the identified relevant parameters to the peak acceleration amplification ratio. Artificial neural networks are useful tool for these two tasks. This statistical learning method can lead to relationships between outputs and a set of input parameters, without any *a priori* assumption on their functional forms. For these two main reasons, artificial neural networks proved to be more and more widespread, they have been used in particular for several applications in the study of site effects (Giacinto et al., 1997, Paolucci et al.,

2000, Boudghene-Stambouli et al., 2017, 2018). The relationships between inputs and outputs are obtained through a "learning phase"during which the network is trained on a set of known data (inputs and corresponding outputs are given to the network) in a way that the network is later able to predict outputs from new inputs that stay in the same area of the parameter space as sampled by the training set. In this work, a particular, very common, architecture of neural network - one of the most common - is considered: the multilayer peceptron.

4.1 *Development of predictive models*

The input parameters for each predictive model have to be representative of the physical mechanisms that determine the value of the output parameters $\frac{a_{crest_{max}}}{\widehat{PGA}}$ and $\frac{a_{block_{max}}}{\widehat{PGA}}$. This representativeness can be evaluated by assessing the performance of each predictive model, that is, its ability to predict target output values. However, performance is not the only criterion: the number of input parameters has to be limited and their correct sampling in the learning dataset has to be ensured in order to avoid overfitting of the predictive models. A procedure of early-stopping is used in order to prevent overfitting (see Durand(2018) for more details). Additionally, the application of a predictive tool to realistic cases requires that its input parameters can be easily estimated. In the end, the difficulty in the design of a predictive model lies in the compromise between its performance and its complexity.

As a performance indicator of our predictive models, we use the Root Mean Square Error *(RMSE)* with respect to the initial standard deviation on the target output values. The Root Mean Square Error corresponds to the standard deviation of the differences between the outputs of the neural network and the target values from the whole dataset, as defined in the following equation:

$$RMSE = \sqrt{\frac{1}{N}\sum_{k=1}^{N}(t_k - o_k)^2} \tag{3}$$

where N is the number of samples in the learning dataset (equal in this study to 540 or 2700 depending on whether the research result is $a_{crest_{\max}}$ or $a_{block_{\max}}$), t_k is the value of the target for the sample number k and o_k the respective output from the neural network. A high reduction of the standard deviation corresponds to a high performance of the network and, in particular, it means that the chosen input parameters are able to explain the target output values.

The best combinations of input parameters are identified thanks to an iterative methodology that can be best illustrated by the example of the selection of input parameters for the prediction of $\frac{d_{crest_{max}}}{\widehat{PGA}}$. The results presented in Figure 3 show the effects of the velocity contrast $V_d/\hat{V}_c$, of the ratio of "thicknesses" H_c/H_d and of $\widehat{PGA}$ on the value of $\frac{a_{crest_{max}}}{\widehat{PGA}}$ However, the use of these three parameters as inputs of a neural network for the prediction of $\frac{a_{crest_{max}}}{\widehat{PGA}}$ turned out to be less satisfactory. Moreover, non-linearity should be more correlated with shear strain than with the only value of $\widehat{PGA}$. Additionally, as the latter takes only four values in our dataset (0.0981 m/s^2, 0.981 m/s^2, 2.943 m/s^2 and 4.905 m/s^2), it cannot guarantee a relevant sampling. Therefore, other more relevant parameters or combinations of parameters have to be tested. A conceivable proxy for peak shear strain in the soil layer can be PGV/Vs_{30} (Idriss, 2011) where PGV is the peak ground velocity (top of the layer) and V_{S30} the mean shear wave velocity over the thirty first meters of soil. This proxy does not use parameters of the numerical model, but one can approximate PGV by $\widehat{PGA}$ divided by the fundamental pulsation of the layer, and then assume that these pulsation is proportional to $\hat{V}_c/H_c$ and finally one can replace VS_{30} by $\hat{V}_c$ in order to obtain the following proxy for peak deformation in the layer: $\frac{\widehat{PGA}\,H_c}{\hat{V}_c^{\,2}}$. The use of $V_d/\hat{V}_c$, H_c/H_d and $\frac{\widehat{PGA}\,H_c}{\hat{V}_c^{\,2}}$ as input parameters of a new neural network

leads to a better performance. Adding a fourth input parameter for other tests of neural network models proved to introduce more complexity without any substantial gain in the accuracy of predicted target values. Finally, it must be noticed that the input parameters mentioned above use information that are not always easily measurable. The minimal shear wave velocity at top of the layer $V_{c_{min}}$. and the fundamental resonance frequency of the layer f_0 (which is more or less proportional to $\hat{V}_c/H_c$) are much easier to obtain (see measurements on small embankments presented in Durand 2018), we therefore choose to replace $\hat{V}_c$ by V_{cmin} and H_c by V_{cmin}/f_0 in the previous input parameters in order to develop an easy-to-use predictive model. Finally, because our target output parameters are ratios, it is better to use their logarithmic values. The iterative methodology detailed above leads to the identification of the following combinations of parameters and respective neural network:

- Network ANN1 with inputs $\ln(V_d/Vc_{mm})$, $\ln(V_{c_{\min}}/(H_d f_o))$, and $\ln\left(\widehat{PGA}/(V_{c_{\min}}f_o)(V_{c_{\min}}f_o)\right)$ for the prediction of $\ln\left(a_{crest_{max}}/\widehat{PGA}\right)$
- Network ANN2 with inputs $\ln(V_d/Vc_{mm})$, $\ln(V_{c_{\min}}/(H_d f_o))$, $\ln\left(\widehat{PGA}/(V_{c_{\min}}f_o)(V_{c_{\min}}f_o)\right)$ and $\ln(yb/Hd)$ for the prediction of $\ln\left(a_{block_{max}}/\widehat{PGA}\right)$.

The value of *RMSE* obtained for the prediction of $\ln\left(a_{crest_{max}}/\widehat{PGA}\right)$ is equal to 0.15, which corresponds to a reduction of 80% of the initial standard deviation. The neural network can predict the value of $\ln\left(a_{crest_{max}}/\widehat{PGA}\right)$ with a precision of 16%. As shown on Figure 4(a), the correlation between the outputs of the neural network and the targets of the dataset (results from numerical simulation) is satisfactory. The 16% precision is reported with the dashed lines on this same figure. Regarding the prediction of $\ln\left(a_{block_{max}}/\widehat{PGA}\right)$, the developed neural network leads to a value of *RMSE* equal to 0.15 also, that corresponds to a slightly lower reduction of the initial standard deviation (74%). The precision on the prediction is again equal to 16%. The correlation between the outputs of the neural networks and the results of numerical simulations is displayed in Figure 4(b)M.

4.2 *A use of the models: Representation of abacus*

The developed neural network are easy-to-use tools for the direct prediction of peak acceleration at crest and of possible sliding blocks: they can directly link the researched outputs from known inputs through a relation that can be implemented in any spreadsheet. However, in order to provide a more visual tool to the engineering community and to validate the behavior of the models some abacus are developed. An example of representation of the results provided by the network ANN1 for the prediction of $\frac{a_{crest_{max}}}{\widehat{PGA}}$ is given on Figure 5. The outputs of the network are represented with a colorscale in the plane formed by two of the inputs

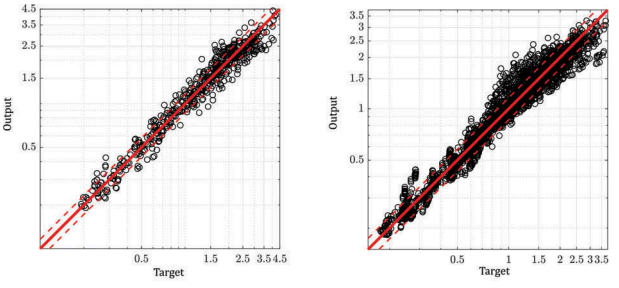

(a) Prediction of $\frac{a_{crest_{max}}}{\widehat{PGA}}$ with the neural netwkork ANN1.

(b) Prediction of $\frac{a_{block_{max}}}{\widehat{PGA}}$ with the neural netwkork ANN2.

Figure 4. Correlations between the outputs of the neural networks used to predict (a) $\frac{a_{crest_{max}}}{\widehat{PGA}}$ and (b) $\frac{a_{block_{max}}}{\widehat{PGA}}$ and the targets (that correspond to data from numerical simulations).

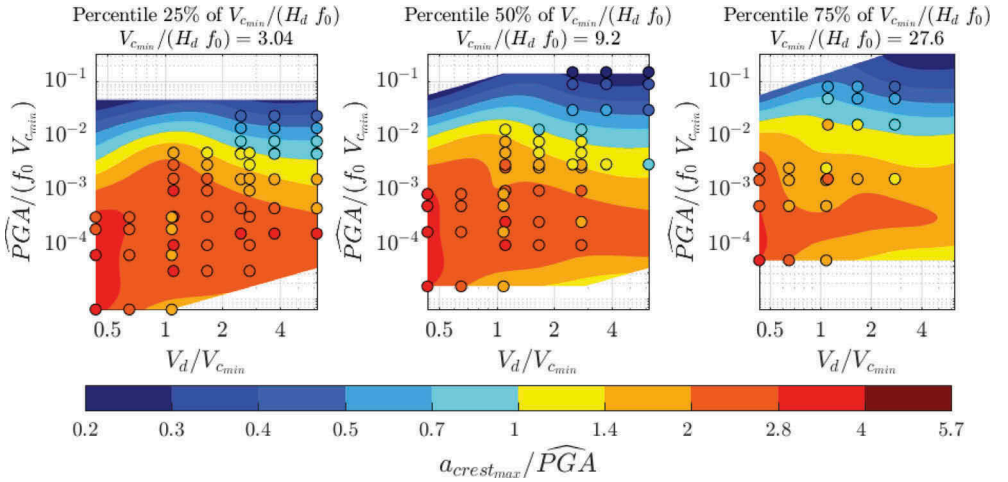

Figure 5. Abacus for estimation of amplification at crest with respect to outcropping bedrock ($a_{crest_{max}}/PGA$). Outputs of the dedicated neural network in the plane formed by $V_d/V_{C_{min}}$ and PGA/(V_{Cmin} f_0) for three different percentiles of $V_{C_{min}}/(H_d f_0)$: 25% (left), 50% (middle) and 75% (right). The circles o with the same colorscale represents the numerical data from SPECFEM 2D.

$\left(V_d/V_{c_{min}}\ and\ \widehat{PGA}/(f_0\ V_{c_{min}})\right)$and for a fixed value of the third input $V_{c_{min}}/(f_0 H_d)$equal to 3.04 (25% percentile) on the left, 9.2 (median) in the middle and 27.6 (75% percentile) on the right. In order to compare the outputs of the neural network and the numerical results, the latter are represented in the same plane with circles colored with the same colorscale. The location of the numerical data has also the advantage to show the space of input parameters where numerical results are valid (one can be confident in the outputs of the neural network only in areas where learning data are available). This representation confirms the relatively good precision of the predictions made by the ANN1 network.

5 CONCLUSIONS

The main contribution of this work is to propose new predictive models to assess peak acceleration at crest of an embankment and peak acceleration of a potentially sliding blocks which are both relatively simple (the corresponding mathematical relationships can be implemented in any spreadsheet with a reduced number of easy to measure inputs) and based on realistic numerical models (that take into account the presence of a natural soil layer and a correct dissipation of energy).

Artificial neural networks proved to be a very useful tool to derive simple relationships from the numerical results. Two neural networks are developed in this work. The first one provides the value of peak acceleration at crest of an embankment knowing only a limited set of easily affordable parameters. The final dimensionless parameters required for the prediction are a velocity contrast indicator V_d/V_{cmin}, a thickness ratio proxy $V_{cmin}/(H_d\ f_0)$ and a strain proxy $\widehat{PGA}/(V_{c_{min}} fo)$. The required parameters are thus the thickness and shear wave velocity of the embankment (V_d), the minimum shear wave velocity in the foundation soil ($V_{c_{min}}$), the soil fundamental frequency (f_o), and the design PGA for outcropping bedrock. The second neural network leads to the prediction of peak acceleration of potentially sliding blocks, with an additional information about the geometry of the block through a fourth input y_b/H_d where y_b is the thickness of the block. Both models are very satisfactory with a precision of 16% on the research result. Abacuses are also developed using these prediction models to provide a more visual tool to the engineering community. This representation is also very useful to identify the space where input parameters are valid and to visualize the main trends.

In order to develop a simplified approach, many assumptions have been made in the elaboration of the numerical models which impact on peak acceleration could be evaluated, by comparing for example on a few cases the obtained results with results from complete nonlinear computations. Other degradation curves could also be used for linear equivalent simulations, with a different plasticity index. Moreover, artificial neural networks could be used to increase the value of the 1D linear equivalent computations performed within this work. In the long term, the most interesting prospect of this work would be to compare results given by this simplified approach to instrumental data recorded on real embankment sites.

ACKNOWLEDGMENTS

This work has been carried out within the framework of a"CIFRE" PhD grant 2015/029 from the"ANRT" (Association franaise Recherche Technologie), awarded through the company"-Geo- phyconsult SAS" (Chambry, France) with the funding support of EDF-CIH (Electricit de France, Chambry, France) and CNR (Compagnie Nationale du Rhne, Lyon, France). The spectral element computations presented in this paper were performed using the Froggy platform of the CIMENT infrastructure (https://ciment.ujf-grenoble.fr), which is supported by the Rhône-Alpes region (GRANT CPER07_13 CIRA), the 0SUG@2020 labex (reference ANR10 LABX56) and the Equip@Meso project (reference ANR-10-EQPX-29-01) of the programme Investissements d'Avenir supervised by the Agence Nationale pour la Recherche.

REFERENCES

Akkar, S. et al. 2014. Reference database for seismic ground-motion in Europe (RESORCE). *Bulletin of Earthquake Engineering* 12(1):311-339.

Boudghene-Stambouli, A., Zendagui, D., Bard, P.-Y. and Derras, B., 2017. Deriving amplification factors from simple site parameters using generalized regression neural networks: implications for relevant site proxies. *Earth, Planets and Space* 69-99.

Boudgene-Stambouli, A., P.-Y. Bard, E. Chaljub, P. Moczo, J. Kristek, S. Stripajova, C. Durand, D. Zendagui and B. Derras, 2018. 2D/1D Aggravation Factors: From A Comprehensive Parameter Study To Simple Estimates With A Neural Network Model. 16ECEE (16th European Conference on Earthquake Engineering), Thessaloniki, Greece, June 18-21, 2018, paper 624, 12 pages.

Causse, M., Laurendeau, A., Perrault, M., Douglas, J., Bonilla, L. F., Guguen, P. 2014. Eurocode 8-compatible synthetic time-series as input to dynamic analysis. *Bulletin of Earthquake Engineering* 12 (2):755-768.

Darendeli, M. B. 2001. Development of a new family of normalized modulus reduction and material damping curves. PHD thesis. The University of Texas at Austin.

Durand, C., Chaljub, E., Bard, P.-Y., Baillet, L., Fry, J.-J., Granjon, R., Renalier, F. 2017. Revisiting Sarma's method for seismic response of embankments: first results. 16th World Conference on Earthquake Engineering, Santiago, Chili.

Durand, C. 2018. Stabilite des digues sous chargement sismique: vers une nouvelle generation de methodes simplifiees. PHD thesis, Universite de Grenoble Alpes.

Giacinto, G., Paolucci, R., Roli, F. 1997. Application of neural networks and statistical pattern recognition algorithms to earthquake risk evaluation. *Patter Recognition Letters*.

Idriss, I. M., Sun, J. I. 2012. User's manual for SHAKE91.

Martin, R., Komatitsch, D., Blitz, C., Le Goff, N. 2008. Simulation of seismic wave propagation in an asteroid based upon an unstructured MPI spectral-element method: Blocking and non-blocking communication strategies. Lecture Notes in Computer Science (including subseries Lecture Notes in Artificial Intelligence and Lecture Notes in Bioinformatics).

Paolucci, R., Colli, P., Giacinto, G. 2000. Assessment of seismic site effects in 2-D alluvial valleys using neural networks. *Earthquake Spectra* 16(3):661-680.

Sarma, S. K. 1979. Response and Stability of Earth Dams during Strong Earthquakes.U.S. Army Engineer Waterways Experiment Station Geotechnical Laboratory.